Journal of *Marine Science and Engineering*

MDPI

Article

Frazil Ice in the Antarctic Marginal Ice Zone

Felix Paul [1], Tommy Mielke [1], Carina Schwarz [2], Jörg Schröder [2], Tokoloho Rampai [3,4], Sebastian Skatulla [4,5], Riesna R. Audh [4,6], Ehlke Hepworth [4,6], Marcello Vichi [4,6] and Doru C. Lupascu [1,*]

1 Institute for Materials Science and Center for Nanointegration Duisburg-Essen (CENIDE), University of Duisburg-Essen, 45141 Essen, Germany; felix.paul@uni-due.de (F.P.); tommy.mielke@uni-due.de (T.M.)
2 Institute of Mechanics, University of Duisburg-Essen, 45141 Essen, Germany; carina.schwarz@uni-due.de (C.S.); j.schroeder@uni-due.de (J.S.)
3 Department of Chemical Engineering, University of Cape Town, Rondebosch 7701, South Africa; tokoloho.rampai@uct.ac.za
4 Marine and Antarctic Research Centre for Innovation and Sustainability, University of Cape Town, Cape Town 7700, South Africa; sebastian.skatulla@uct.ac.za (S.S); ADHRIE001@myuct.ac.za (R.R.A.); djnehl001@myuct.ac.za (E.H.); marcello.vichi@uct.ac.za (M.V.)
5 Department of Civil Engineering, University of Cape Town, Rondebosch 7701, South Africa
6 Department of Oceanography, University of Cape Town, Cape Town 7701, South Africa
* Correspondence: doru.lupascu@uni-due.de; Tel.: +49-201-183-2737

Abstract: Frazil ice, consisting of loose disc-shaped ice crystals, is the first ice that forms in the annual cycle in the marginal ice zone (MIZ) of the Antarctic. A sufficient number of frazil ice crystals form the surface "grease ice" layer, playing a fundamental role in the freezing processes in the MIZ. As soon as the ocean waves are sufficiently damped by a frazil ice cover, a closed ice cover can form. In this article, we investigate the rheological properties of frazil ice, which has a crucial influence on the growth of sea ice in the MIZ. An in situ test setup for measuring temperature and rheological properties was developed. Frazil ice shows shear thinning flow behavior. The presented measurements enable real-data-founded modelling of the annual ice cycle in the MIZ.

Keywords: marginal ice zone; Antarctic; frazil ice; sea ice; grease ice; rheology; viscosity

Citation: Paul, F.; Mielke, T.; Schwarz, C.; Schröder, J.; Rampai, T.; Skatulla, S.; Audh, R.R.; Hepworth, E.; Vichi, M.; Lupascu, D.C. Frazil Ice in the Antarctic Marginal Ice Zone. *J. Mar. Sci. Eng.* **2021**, *9*, 647. https://doi.org/10.3390/jmse9060647

Academic Editor: Michael Meylan

Received: 6 May 2021
Accepted: 7 June 2021
Published: 10 June 2021

1. Introduction

The growth and melting of sea ice in the Antarctic polar region represents one of the largest seasonal changes on Earth [1]. These seasonal variations are of greatest importance for the bio-habitat of Antarctica as well as for the global climate. However, the seasonal and long-term variability of sea ice extent in the marginal ice zone (MIZ) of the Antarctic is poorly understood and not captured by current climate models [2]. Frazil ice, which consists of loose disc-shaped ice crystals formed in turbulent and supercooled water, plays a key role in this freezing process in the MIZ of the Antarctic. The MIZ is the transition zone between open water and consolidated ice where the sea ice concentration is between 15% and 80%. When a sufficiently large quantity of frazil ice is present, it clusters to form agglomerations of ice, which later form into pancake ice. These pancakes grow and a frazil/pancake mixture develops, where the frazil ice acts as a binder between the pancakes [3]. Large incident ocean waves lead to fracture, overtopping, and rafting of pancakes in the high wave energy regime closer to the open water edge of the MIZ [4]. As soon as the waves are sufficiently attenuated by this frazil/pancake layer, a consolidated ice cover can form. This process is denoted as the pancake ice cycle [5].

Frazil ice crystals are simple in their shape, appearing as thin, circular, disc-shaped crystals, due to the higher growth rate within the basal plane of the hexagonal crystal lattice of ice [6]. The crystals tend to have a diameter of between 0.01 mm and 5 mm and their thickness varies between 1 µm and 100 µm [7,8]. Frazil ice crystals can only develop under turbulent and supercooled conditions [8]. Turbulence, induced by wind and wave

energy, is necessary for the nucleation of crystals from the supercooled water as well as for the ongoing frazil ice production [9]. Stronger turbulence leads to a higher particle collision rate and, therefore, to faster frazil production. During freezing, salt ions are hardly incorporated into the ice lattice and are thus rejected from the ice into the water [10]. When the frazil ice concentration increases, it appears as a milky grey layer at the surface. This layer of "grease ice" consists of water and frazil ice crystals [11].

There is still a lack of knowledge about sea ice dynamics in the MIZ, in which ocean waves play a key role, in particular at the scale of a wave length [12]. It is known that wave attenuation is significantly correlated with ice conditions [13–15], including the wavelength to floe size ratio [16], and thus with ice properties, such as ice thickness, strength, and viscosity [17–19]. However, there are few data available on ice properties in the MIZ of the Antarctic [20].

This study investigates the properties of frazil ice, encompassing temperature and its rheological properties. The latter are essential for numerical simulations of sea ice dynamics in the Antarctic MIZ. The temporal and spatial evolution of sea ice and coupled wave attenuation are influenced by damping effects due to interstitial frazil ice and the complex pancake ice floe collision dynamics, including dissipative effects, such as friction, ridging, and rafting [21], as well as eddy viscosity in the turbulent boundary layer [22,23]. The hydrodynamics of interstitial frazil ice and its interaction with pancake ice floes in terms of form drag are key aspects in wave energy dissipation [24]. Therefore, a sufficiently precise description of the rheological properties of frazil ice is essential.

Viscosity in an open system such as the ocean surface is a complex matter. In this work, we focus on the local scale, namely a few centimeters to roughly 50 cm. Obviously, there is a scale beneath which the interaction of single ice crystals is relevant, and this would be the subject of a micro-viscosity study. On a scale larger than our measurements, the frazil ice is a damping component in the setting of floe plus frazil ice. Under high agitation, viscosity will again be changed due to the direct interaction of floes with each other by impact and by breakup of rafts [25]. The largest scale concerns wave attenuation on the 100 m to 100 km scale where completely effective media values come into play, which ultimately determine the interaction of the ice field with the atmosphere on a global scale [26]. At this point we cannot say how the different scales are interlinked, but we provide in situ data on the centimeter to 0.5 m scale to build models upon.

No in situ measured rheological properties of grease ice or frazil ice can be found in the literature; only measurements in wave tanks [27–30] and the Arctic [14] have been recorded. The viscosity of the sea ice layer has also been derived on the basis of SAR images in the Antarctic [31] and a combination of buoy and SAR measurements in the Arctic [32]. Most studies available focus on the effect of frazil ice on wave damping [23,33] but do not focus on the rheological properties of frazil ice itself. Our study specifically focuses on in situ data collected during the SCALE (http://scale.org.za) Winter Cruise in July 2019 to the MIZ of the Antarctic. The results are compared to literature values.

2. Materials and Methods

The experiments were conducted on the South African research vessel SA Agulhas II during the SCALE Winter Cruise 2019. Frazil ice was collected at three stations, termed MIZ1s on the 26th of July, MIZ2 on the 27th of July, and MIZ1n on the 28th of July. The frazil ice sample was lifted out of the water with a custom-built frazil ice sampler (Figure 1III). The viscosity of the specimen was measured with an eBT-V rheometer (Schleibinger Testing Systems, Buchbach, Germany).

The frazil ice sampler (Figure 1III) is similar in design to a Niskin bottle. It enables the retrieval of an undisturbed frazil ice specimen. The sampler consists of a metal cylinder, which is moveable along four steel bars between two fixed metal plates. The metal cylinder acts as the wall of a bucket. A foam mat attached to the bottom metal plate acts as a seal when the cylinder is placed on top of it, forming a water-tight bucket preventing water from draining out. Before lowering the frazil sampler into the water, the cylinder was

pulled up to the top plate via the green ropes shown in Figure 1IIIf where it was held before sampling. Once the sampler was lowered into the frazil ice layer with the yellow mark touching the ocean (Figure 1IIIj), it was moved horizontally with the help of guidance lines to a position where the ice was undisturbed. Then, the cylinder was carefully lowered to the bottom plate and shut by pulling the red ropes (see Figure 1IIIf). It was then lifted on board, yielding an undisturbed frazil ice sample.

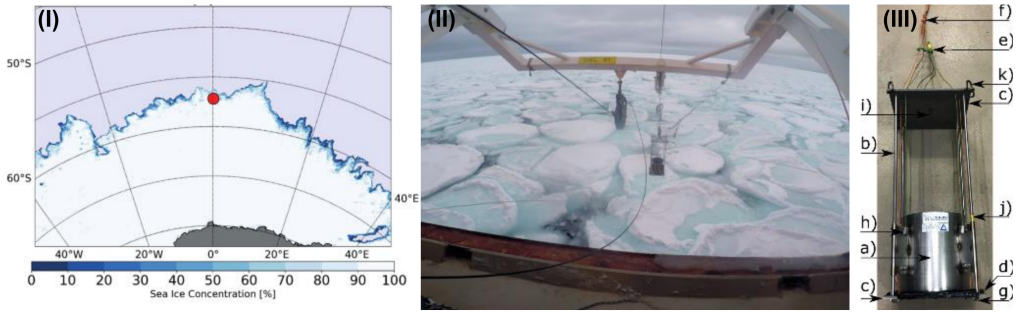

Figure 1. (**I**) Map showing the sea ice condition on the 28 July 2019; the red dot on the map shows the positions of the vessel. ASI Algorithm AMSR2 sea ice concentrations were obtained for 28 July 2019 from the Integrated Climate Date Center (ICDC, icdc.cen.uni-hamburg.de/), University of Hamburg, Hamburg, Germany [34,35]. (**II**) Picture of the actual sea conditions. (**III**) Sketch of the frazil ice sampler for the retrieval of an undisturbed sample consisting of (a) metal cylinder $h_c = 280$ mm, $r_c = 135$ mm; (b) four steel bars; (c) two metal plates; (d) foam mat; (e) rope to open the sampler; (f) rope to close the sampler; (g) loop for rope; (h) bolts to fasten rope; (i) hook; (j) yellow mark; (k) hooks.

On the deck of the ship, the temperature of the frazil ice sample was measured immediately. Subsequently the viscosity was tested in the same sampling bucket using a vane rheometer (Figure 2). The vane has a radius of R_V = 51.5 mm and a height of H = 103 mm (Figure 2). The viscosity test lasted 60 s linearly ramping up from an initial rotation speed of $\omega = 1\frac{rev}{min}$ up to $\omega = 10\frac{rev}{min}$. The collected data allow the determination of the shear stress τ (Equation (1)), shear rate $\dot{\gamma}$ (Equation (2)), and viscosity η (Equation (3)) of every sample based on the measured resistance torque M:

$$\tau = \frac{M}{2\pi R_V^3}\left(\frac{H}{R_V} + \frac{2}{3}\right)^{-1} \quad (1)$$

$$\dot{\gamma} = \frac{4\pi R_S^{2/n}}{\left({R_S}^{2/n} - {R_V}^{2/n}\right)}\frac{\omega}{\mathrm{n}} \quad (2)$$

$$\eta_{\mathrm{aparent}} = \frac{\tau}{\dot{\gamma}} \quad (3)$$

Equation (1) allows the calculation of the shear stress from the measured torque and takes the effect at the end surfaces of the vane into account [36]. Equation (2) allows the calculation the shear rate for power law fluids with the flow behavior index n [37]. As a shear thinning behavior is expected for frazil ice, the flow behavior index is set to $n = 0.5$ comparable to the Casson fluid model. This is an estimated value that displays the non-Newtonian behavior of the fluid and must be confirmed by the data. Immediately after the viscosity measurement was taken, the collected frazil ice was separated into its two components, pure frazil ice crystals and salt water, for further testing of the individual constituents. This separation was achieved by opening the frazil sampler and allowing the frazil ice to flow through a cotton sheet into a box, after which the cotton sheet held the pure frazil ice crystals and the salt water was inside the box.

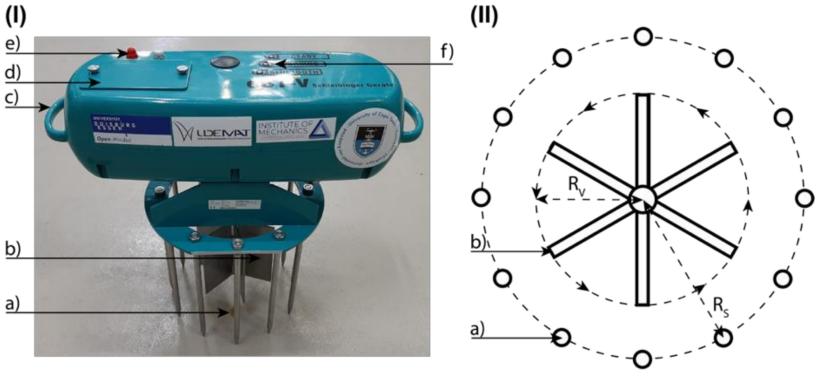

Figure 2. Picture (**I**) and drawing (**II**) of the rheometer: (a) steel bars; (b) vane; (c) handle; (d) battery case; (e) switch; (f) control lights.

3. Results

During the cruise, twelve frazil ice samples were collected. The volumes of the ice samples varied between 11.2 dm^3 and 16 dm^3. The highest pure frazil ice crystals weight percentage in the sample was calculated for MIZ2 at 22:10 h with 40% frazil, the lowest at MIZ2 21:35 h with 16% frazil. The large variation of the frazil ice concentrations at MIZ2 showed that the frazil ice was not equally distributed between the pancakes, reflecting continuous spatial and temporal changes.

While the frazil ice concentration varied, the sample temperature was constant over all stations at −1.90 °C and was practically not affected by the outside temperature, which varied between −4.4 °C and −18.9 °C. Wind speeds at the three stations ranged between Beaufort scale 2 and 4 and indicated that the remaining incident wave energy additionally sustained by the wind forcing introduced enough turbulence in the water for continued frazil ice production. This corresponds to the findings of Smedsrud [38] in the Arctic region that a wind speed of 10 m/s is sufficient to form a 30 cm frazil ice layer.

Figure 3 shows the shear stress and the apparent viscosity of ten frazil ice samples collected at MIZ1s, MIZ2, and MIZ1n; two samples are not displayed because they did not show a noteworthy shear stress. The shear stress curves are fitted with the Herschel–Bulkley model (Equation (4)).

$$\tau = \tau_0 + k\dot{\gamma}^n \tag{4}$$

$$\eta_{\text{apparent}} = r\dot{\gamma}^m \tag{5}$$

All curves in Figure 3 show the shear thinning behavior of the sample. A rotation of the vane of 1/6th of a full turn ($\hat{=}60°$) is completed after 6.66 s, i.e., at a shear rate of 0.96 $\frac{1}{s}$. The rotation by 1/6th of a full turn is important, because at this time, all vanes are one geometrically equivalent position further than the starting point. After all initial bonds in the sample are broken, which is assumed to be the case after 1/6th rotation of the vane, the ice crystals rearrange as with other dispersions [39]. It is assumed that, after reordering, it is mostly water that is shearing in the gap between the rotating cylinder and the outer frazil ice layer. The shear stress graphs in the left column of Figure 3 can be separated into three phases. The first phase is characterized by an increase in shear stress due to mutual hooking of the crystals. When the entangled crystals and larger frazil ice crystals are loosened, it is followed by a second phase, which is seen as a decrease in shear stress. In the third phase, shear stress slowly increases. Mostly water is shearing in the shear zone, combined with friction between the crystals, leading to shear stresses between 25 Pa and 50 Pa in the third phase. This fits with the Herschel–Bulkley model (Equation (4)), and $n = 0.5$ well represents the shear stresses in the third phase; hence, $n = 0.5$ is a suitable value for frazil ice for this shearing scenario.

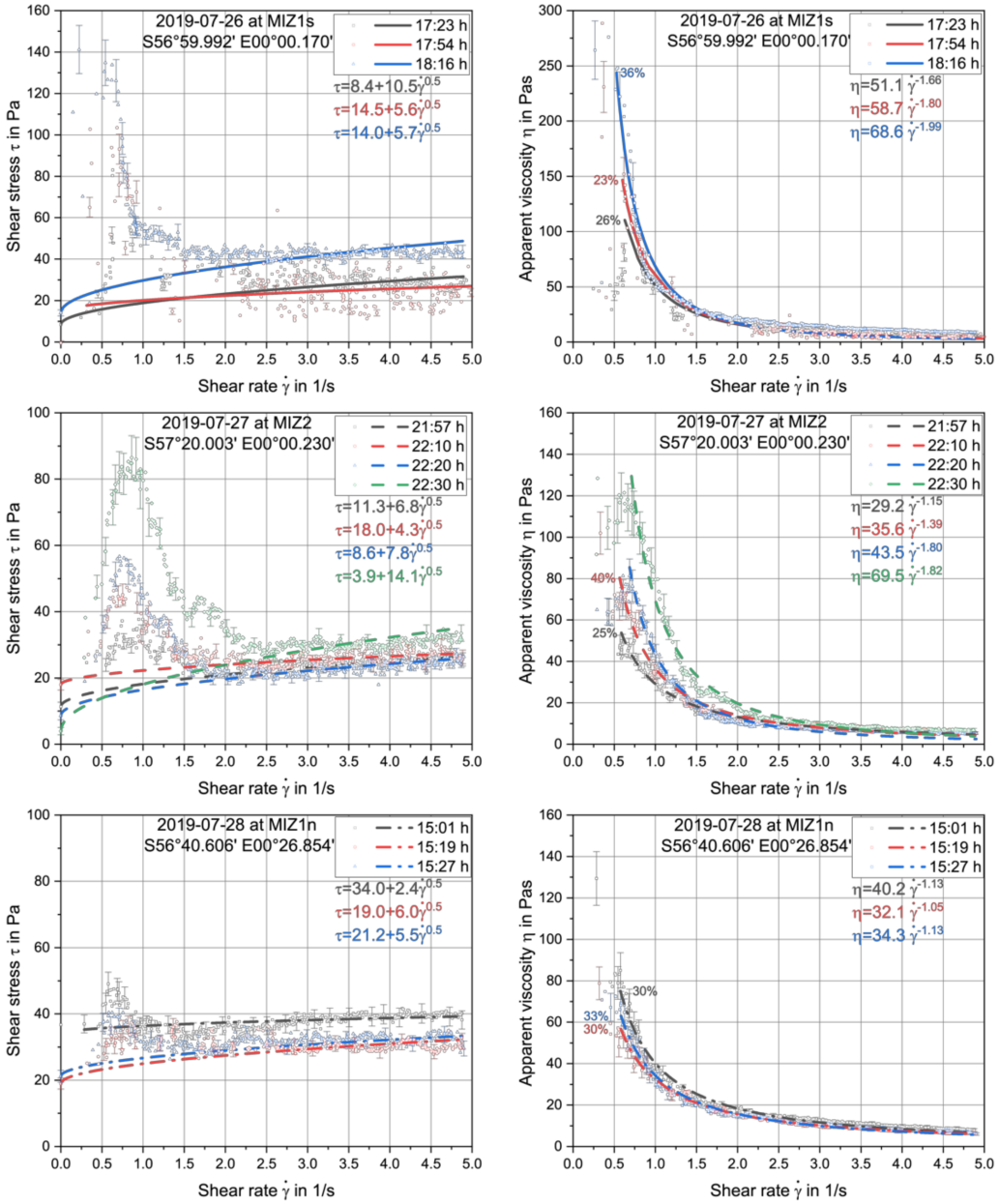

Figure 3. Left column displays the shear stress, and right column displays apparent viscosity at MIZ1s, MIZ2, and MIZ1n. The data set label equals the sampling time. The percentage of frazil ice in weight percent in the samples is given. The displayed error bars are valid for all data points in their vicinity. The error is calculated by estimated maximum deviations of $\Delta R_V = 0.5$ mm, $\Delta R_S = 0.5$ mm, $\Delta M = 1/150 \cdot M + 0.0073$, $\Delta H = 1.0$ mm, and $\Delta\omega = 0$.

The apparent viscosity fits presented in the right column of Figure 3 describe the crystal entangling and shearing of water and frazil ice crystals in the shear zone, without describing the initial increase in viscosity due to hooking of the crystals. Therefore, the parameter m in Equation (5) does not fit the boundaries of $0 < m < 1$ but describes the unmixing of the ice crystals. The apparent viscosity graphs in the right column of Figure 3 descend towards zero for higher shear rates independent of the frazil ice concentration. The highest apparent viscosity at MIZ1s is shown in the curve for 18:16 h; this sample also contained the highest percentage of frazil ice. The fitting curve at MIZ1s for 17:54 h lies above the fitting curve for 17:23 h, even though the percentage of frazil ice is lower for sample 17:54 h. This trend cannot be confirmed by the measurements at MIZ2 (Figure 3). The curve from 22:10 h with 40% frazil ice overlaps with the curve of 21:57 h with 25%

frazil ice. The measurement from MIZ1s for 17:23 h shows an increase in apparent viscosity until a maximum is reached at 275 Pas. This can be explained by a short period of shear thickening in the second phase, where the frazil ice particles strongly interact with each other due to local pile-up of ice crystals in certain volumes in between the vane blades, which leads to a higher apparent viscosity before the shear thinning behavior sets in [40]. The samples from station MIZ1n show the same behavior as that of the samples from MIZ1s (Figure 3). The average percentage of frazil ice in the sample is very similar for all three samples; therefore the apparent viscosity values barely differ.

4. Discussion

Previous publications calculated the viscosity of frazil ice or the viscosity of a frazil and pancake ice system by measuring wave propagation through laboratory tanks, by SAR images on a large scale in the Antarctic, or a combination of buoy and SAR in the Arctic combining different scales. Newyear and Martin obtained viscosity values between 15 ± 0.3 Pas and 30 ± 0.6 Pas [27]; Wadhams et al. obtained a viscosity of 50 ± 1 Pas [31]; Wang and Shen calculated viscosities between 20 ± 0.4 Pas and 60 ± 1.2 Pas [28]; Rabault et al. obtained a viscosity of 9.5 ± 0.5 Pas [14]; and Zhao and Shen calculated the viscosity to be 14 ± 0.3 Pas [29].

The viscosity calculated by Zhao and Shen [29] and Rabault et al. [14] is at the lower end of the range obtained in our measurements. This apparent viscosity was measured at MIZ1s for shear rates greater than $3.00\frac{1}{s}$; at MIZ2 for shear rates greater than $2.50\frac{1}{s}$; and at MIZ1n for shear rates greater than $2.75\frac{1}{s}$. Therefore, data from the Winter Cruise agree with the findings by Zhao and Shen on the low viscosity end of our data [29]. The viscosity values obtained by Wang and Shen [28], Newyear and Martin [27], and Wadhams et al. [31] fit well with the data from our experiments. All stations show apparent viscosity values in this range between shear rates from $1.00\frac{1}{s}$ to $3.50\frac{1}{s}$. Conversely, the data presented in this study suggest that higher viscosities of up to 150 to 300 Pas can be reached when the shear rate, respectively the ocean, is calm.

In order to be able to judge whether the measurements with the rheometer and measurements in a wave tank on artificial sea ice can be compared, the differences between the methods must be highlighted. When measuring the viscosity with a rheometer, an initially undisturbed sample is analyzed by rotating the vane in the sample and recording the torque. The viscosity can then be calculated from the torque using proven formulas from other fields (Equations (1)–(3)). During the rotation of the vane, the internal structure of the frazil ice is rearranged. In contrast, for measurements in the wave tank, the ice is assumed to be a layer on the water in which the internal structure is undisturbed. Therefore, measurement with a rheometer also detects structural changes within the sample. An advantage of measuring with a rheometer is that samples can be specifically selected. With the frazil ice sampler, it was possible to collect samples between the pancakes and measure them afterwards. Attention was also paid to the correct scale of the measurement geometry and the frazil sampler. A smaller measuring device could have been blocked by ice chunks in the sample; larger measurements or other measuring methods always measure the influence of the pancakes on the viscosity. Despite the differences described, the measured viscosities are in the same range of values for the rheometer and measurements in wave tanks.

Shear thinning behavior obtained in the field means that under light swell, the sea ice acts more like consolidated or pack ice, comparable to a film on the water, even though pancakes still drift freely in the ocean [41], whereas under stormy conditions, the frazil ice between the pancakes is less viscous, and this allows the pancakes to drift independently. It is also assumed that the low viscosity under high shear rate supports the air–water interaction during storms, enhancing the formation of new frazil ice.

5. Conclusions

This paper gives a brief overview of the importance of frazil ice for the growth of Antarctic sea ice, which plays a key role in global warming. Measurements of temperature, shear stress, and apparent viscosity were conducted during the Winter Cruise 2019 and constitute the first data set on frazil ice from the Antarctic MIZ ever taken in situ. Results are shown for three stations and twelve samples. Shear-rate-dependent apparent viscosity graphs were fitted. All samples showed shear thinning behavior. The values from the Winter Cruise compared well to literature values which were measured indirectly from wave propagation characteristics in the laboratory. The shear thinning behavior observed in our experiments illustrate that apparent viscosity values vary greatly between different weather conditions in the Antarctic. This makes further frazil formation an easy scenario for highly perturbed surface waters, while the global pancake field dynamics are dominated by lower shear rates exhibiting much higher overall viscosity values. Our data set enables future modelling approaches to rely on a real data set of the viscosity of frazil ice from the Antarctic MIZ, showing that two fundamentally different viscosity regimes must be considered in models. It may help in furthering our understanding of sea ice growth dynamics. This will improve the reliability of modelling and the understanding of the dynamics of the Antarctic MIZ on the small scale as well as its implications on the larger scale dynamics and the annual freezing–thawing cycle in this remote part of the Earth.

Author Contributions: F.P. and R.R.A. carried out the experiments; F.P. wrote the manuscript with support from D.C.L. and E.H.; T.M. designed the frazil sampler; J.S. and C.S. helped during the cruise and supervised the project; D.C.L., S.S., M.V., and T.R. conceived the original ideas; M.V. provided the opportunity for the cruise; D.C.L. supervised the project. All authors have read and agreed to the published version of the manuscript.

Funding: The SCALE cruises are funded by the South African National Research Foundation (NRF) through the South African National Antarctic Programme (SANAP), with contributions from the Department of Science and Innovation and the Department of Environmental Affairs.

Institutional Review Board Statement: Not applicable.

Informed Consent Statement: Not applicable.

Data Availability Statement: The data sets generated and analyzed during the current study are available from the corresponding author on request.

Acknowledgments: Thanks to Dipl.-Ing. Lothar Gehm for the fruitful discussions.

Conflicts of Interest: The authors declare no conflict of interest.

References

1. Doble, M.J.; Coon, M.D.; Wadhams, P. Pancake ice formation in the Weddell Sea. *J. Geophys. Res. Space Phys.* **2003**, *108*. [CrossRef]
2. Turner, J.; Bracegirdle, T.J.; Phillips, T.; Marshall, G.J.; Hosking, J.S. An Initial Assessment of Antarctic Sea Ice Extent in the CMIP5 Models. *J. Clim.* **2013**, *26*, 1473–1484. [CrossRef]
3. Squire, V.A. Past, present and impendent hydroelastic challenges in the polar and subpolar seas. *Philos. Trans. R. Soc. A Math. Phys. Eng. Sci.* **2011**, *369*, 2813–2831. [CrossRef] [PubMed]
4. Squire, V. Ocean Wave Interactions with Sea Ice: A Reappraisal. *Annu. Rev. Fluid Mech.* **2020**, *52*, 37–60. [CrossRef]
5. Lange, M.A.; Ackley, S.F.; Wadhams, P.; Dieckmann, G.S.; Eicken, H. Development of Sea Ice in the Weddell Sea. *Ann. Glaciol.* **1989**, *12*, 92–96. [CrossRef]
6. Daly, S.F. *International Association for Hydraulic Research Working Group on Thermal Regimes Report on Frazil Ice*; American Society for Testing and Materials: Philadelphia, PA, USA, 1994.
7. Martin, S. Frazil Ice in Rivers and Oceans. *Annu. Rev. Fluid Mech.* **1981**, *13*, 379–397. [CrossRef]
8. McFarlane, V.; Loewen, M.; Hicks, F. Measurements of the evolution of frazil ice particle size distributions. *Cold Reg. Sci. Technol.* **2015**, *120*, 45–55. [CrossRef]
9. Maksym, T.; Stammerjohn, S.E.; Ackley, S.; Massom, R. Antarctic sea ice- A polar opposite? *Oceanography* **2012**, *25*, 140–151. [CrossRef]
10. Eicken, H. From the Microscopic, to the Macroscopic, to the Regional Scale: Growth, Microstructure and Properties of Sea Ice. In *Sea Ice*; Blackwell Science Ltd.: Oxford, UK, 2003; pp. 22–81.
11. De Santi, F.; Olla, P. Limit regimes of ice formation in turbulent supercooled water. *Phys. Rev. E* **2017**, *96*, 043106. [CrossRef]

12. Meylan, M.H.; Bennetts, L.G.; Mosig, J.; Rogers, W.; Doble, M.J.; Peter, M.A. Dispersion Relations, Power Laws, and Energy Loss for Waves in the Marginal Ice Zone. *J. Geophys. Res. Ocean.* **2018**, *123*, 3322–3335. [CrossRef]
13. Meylan, M.H.; Bennetts, L.G.; Kohout, A.L. In situ measurements and analysis of ocean waves in the Antarctic marginal ice zone. *Geophys. Res. Lett.* **2014**, *41*, 5046–5051. [CrossRef]
14. Rabault, J.; Sutherland, G.; Gundersen, O.; Jensen, A. Measurements of wave damping by a grease ice slick in Svalbard using off-the-shelf sensors and open-source electronics. *J. Glaciol.* **2017**, *63*, 372–381. [CrossRef]
15. Kodaira, T.; Waseda, T.; Nose, T.; Sato, K.; Inoue, J.; Voermans, J.; Babanin, A. Observation of on-ice wind waves under grease ice in the western Arctic Ocean. *Polar Sci.* **2020**, *27*, 100567. [CrossRef]
16. Smith, M.M.; Thomson, J. Ocean Surface Turbulence in Newly Formed Marginal Ice Zones. *J. Geophys. Res. Ocean.* **2019**, *124*, 1382–1398. [CrossRef]
17. Sutherland, B.R.; Balmforth, N.J. Damping of surface waves by floating particles. *Phys. Rev. Fluids* **2019**, *4*, 014804. [CrossRef]
18. Squire, V.A.; Montiel, F. Evolution of Directional Wave Spectra in the Marginal Ice Zone: A New Model Tested with Legacy Data. *J. Phys. Oceanogr.* **2016**, *46*, 3121–3137. [CrossRef]
19. Martin, S.; Kauffman, P. A Field and Laboratory Study of Wave Damping by Grease Ice. *J. Glaciol.* **1981**, *27*, 283–313. [CrossRef]
20. Timco, G.; Weeks, W. A review of the engineering properties of sea ice. *Cold Reg. Sci. Technol.* **2010**, *60*, 107–129. [CrossRef]
21. Yiew, L.J.; Bennetts, L.G.; Meylan, M.H.; Thomas, G.A.; French, B.J. Wave-induced collisions of thin floating disks. *Phys. Fluids* **2017**, *29*, 127102. [CrossRef]
22. Herman, A.; Cheng, S.; Shen, H.H. Wave energy attenuation in fields of colliding ice floes—Part 1: Discrete-element modelling of dissipation due to ice–water drag. *Cryosphere* **2019**, *13*, 2887–2900. [CrossRef]
23. Sutherland, G.; Rabault, J.; Christensen, K.H.; Jensen, A. A two layer model for wave dissipation in sea ice. *Appl. Ocean. Res.* **2019**, *88*, 111–118. [CrossRef]
24. Kohout, A.L.; Meylan, M.; Plew, D.R. Wave attenuation in a marginal ice zone due to the bottom roughness of ice floes. *Ann. Glaciol.* **2011**, *52*, 118–122. [CrossRef]
25. Voermans, J.J.; Rabault, J.; Filchuk, K.; Ryzhov, I.; Heil, P.; Marchenko, A.; Iii, C.O.C.; Dabboor, M.; Sutherland, G.; Babanin, A.V. Experimental evidence for a universal threshold characterizing wave-induced sea ice break-up. *Cryosphere* **2020**, *14*, 4265–4278. [CrossRef]
26. Thomson, J.A.L.; Rogers, W. Swell and sea in the emerging Arctic Ocean. *Geophys. Res. Lett.* **2014**, *41*, 3136–3140. [CrossRef]
27. Newyear, K.; Martin, S. Comparison of laboratory data with a viscous two-layer model of wave propagation in grease ice. *J. Geophys. Res. Space Phys.* **1999**, *104*, 7837–7840. [CrossRef]
28. Wang, R.; Shen, H.H. Experimental study on surface wave propagating through a grease–pancake ice mixture. *Cold Reg. Sci. Technol.* **2010**, *61*, 90–96. [CrossRef]
29. Zhao, X.; Shen, H.H. Wave propagation in frazil/pancake, pancake, and fragmented ice covers. *Cold Reg. Sci. Technol.* **2015**, *113*, 71–80. [CrossRef]
30. Rabault, J.; Sutherland, G.; Jensen, A.; Christensen, K.H.; Marchenko, A. Experiments on wave propagation in grease ice: Combined wave gauges and particle image velocimetry measurements. *J. Fluid Mech.* **2019**, *864*, 876–898. [CrossRef]
31. Wadhams, P.; Parmiggiani, F.; de Carolis, G. Wave dispersion by antarctic pancake ice from SAR images: A method for measuring ICE thickness. In Proceedings of the SEASAR 2006 Advances in SAR Oceanography from Envisat and ERS Missions, Frascati, Italy, 23–26 January 2006. no. ESA SP-613.
32. Rogers, W.E.; Thomson, J.; Shen, H.H.; Doble, M.J.; Wadhams, P.; Cheng, S. Dissipation of wind waves by pancake and frazil ice in the autumn Beaufort Sea. *J. Geophys. Res. Ocean.* **2016**, *121*, 7991–8007. [CrossRef]
33. Goldstein, S.; Lamb, H.; Müller, W. Hydrodynamics. *Math. Gaz.* **1933**, *17*, 215. [CrossRef]
34. Kaleschke, L.; Lüpkes, C.; Vihma, T.; Haarpaintner, J.; Bochert, A.; Hartmann, J.; Heygster, G. SSM/I Sea Ice Remote Sensing for Mesoscale Ocean-Atmosphere Interaction Analysis. *Can. J. Remote Sens.* **2001**, *27*, 526–537. [CrossRef]
35. Spreen, G.; Kaleschke, L.; Heygster, G. Sea ice remote sensing using AMSR-E 89-GHz channels. *J. Geophys. Res. Space Phys.* **2008**, *113*. [CrossRef]
36. Dzuy, N.Q.; Boger, D.V. Yield Stress Measurement for Concentrated Suspensions. *J. Rheol.* **1983**, *27*, 321–349. [CrossRef]
37. Steffe, J.F. *Rheological Methods in Food Process Engineering*; Freeman Press: East Lansing, MI, USA, 1992.
38. Smedsrud, L.H. Grease-ice thickness parameterization. *Ann. Glaciol.* **2011**, *52*, 77–82. [CrossRef]
39. Mezger, T. Fittung functions for flow and viscosity curves. In *The Rheology Handbook*; Vincentz Network: Hannover, German, 2009; pp. 59–64.
40. Macosko, C.W. *Rheology: Principles, Measurements and Applications*; Wiley: New York, NY, USA, 1994.
41. Alberello, A.; Bennetts, L.; Heil, P.; Eayrs, C.; Vichi, M.; MacHutchon, K.; Onorato, M.; Toffoli, A. Drift of Pancake Ice Floes in the Winter Antarctic Marginal Ice Zone During Polar Cyclones. *J. Geophys. Res. Ocean.* **2020**, *125*, 1–16. [CrossRef]